NMR Solution Structure of the Glucagon Antagonist [desHis[1], desPhe[6], Glu[9]]Glucagon Amide in the Presence of Perdeuterated Dodecylphosphocholine Micelles[†,‡]

Jinfa Ying, Jung-Mo Ahn,[§] Neil E. Jacobsen, Michael F. Brown, and Victor J. Hruby*

Department of Chemistry, University of Arizona, Tucson, Arizona 85721

Received August 14, 2002; Revised Manuscript Received December 2, 2002

ABSTRACT: Glucagon, a 29-residue peptide hormone, plays an important role in glucose homeostasis and in *diabetes mellitus*. Several glucagon antagonists and agonists have been developed, but limited structural information is available to clarify the basis of their biological activity. The solution structure of the potent glucagon antagonist, [desHis[1], desPhe[6], Glu[9]]glucagon amide, was determined by homonuclear 2D NMR spectroscopy at pH 6.0 and 37 °C in perdeuterated dodecylphosphocholine micelles. The overall backbone root-mean-square deviation (rmsd) for the structured portion (residues 7−29, glucagon numbering) of the micelle-bound 27-residue peptide is 1.36 Å for the 15 lowest-energy structures, after restrained molecular dynamics simulation. The structure consists of four regions (segment backbone rmsd in Å): an unstructured N-terminal segment between residues 2 and 5 (1.68), an irregular helix between residues 7 and 14 (0.79), a hinge region between residues 15 and 18 (0.54), and a well-defined α-helix between residues 19 and 29 (0.33). The two helices form an L-shaped structure with an angle of about 90° between the helix axes. There is an extended hydrophobic cluster, which runs along the inner surface of the L-structure and incorporates the side chains of the hydrophobic residues of each of the amphipathic helices. The outer surface contains the hydrophilic side chains, with two salt bridges (D15-R18 and R17-D21) implied from close approach of the charged groups. This result is the first clear indication of an overall tertiary fold for a glucagon analogue in the micelle-bound state. The relationship of the two helical structural elements may have important implications for the biological activity of the glucagon antagonist.

Glucagon is a 29 amino acid peptide hormone (Figure 1) that is secreted by the α-cells of the pancreas and interacts with specific receptors located in various organs, especially the liver, where it plays a crucial role in glucose homeostasis in mammals. Its primary function is to initiate glucose production by stimulating glycogenolysis and gluconeogenesis in hepatocytes (*1*, *2*) and lipolysis in adipocytes (*3*). In *diabetes mellitus*, a debilitating disease of glucose utilization, hyperglycemia is generally accompanied with an increased level of serum glucagon (*4*, *5*). On the basis of this observation, Unger and Orci have proposed the bihormonal hypothesis (*4*, *5*): insulin deficiency causes impairment of glucose utilization, but overproduction of glucose and ketones by the liver is primarily mediated by glucagon. As a result, numerous glucagon antagonists have been developed to evaluate the role of glucagon in *diabetes mellitus* (*6*−*8*). Several glucagon antagonists, such as [N[α]-trinitrophenyl-His[1], homo-Arg[12]]glucagon (*9*), [desHis[1], Glu[9]]glucagon amide (*10*), and [desHis[1], desPhe[6], Glu[9]]glucagon amide (*11*) (the subject of this study), have been successfully utilized to reduce glucose concentration in vivo (*12*−*14*), and these experiments have opened the door for the possible use of glucagon antagonists as therapeutics.

```
1    5    10   15   20   25
- SQGT - TSEYSKYLDSRRAQDFVQWLMNT-NH2   Glucagon Antagonist
HSQGTFTSDYSKYLDSRRAQDFVQWLMNT         Glucagon
HAEGTFTSNVSSYLEGQAAKEF I AWLVKGR-NH2  GLP-1-(7-35)-NH2
```

FIGURE 1: Sequence alignment of glucagon and glucagon homologues, using glucagon numbering.

It is well-known that glucagon can adopt a variety of conformations depending on the surrounding environment (*15*). Early circular dichroism (CD) measurements found that glucagon exists in at least three conformational states, defined as having high, low, or zero α-helical content. The crystal structure of glucagon shows a helical region corresponding to about 16 residues of α-helix, extended at either end by four residues of less regular, right-handed helix (*16*). The helix is amphipathic with the hydrophobic face of the N-terminal portion (residues 5−14) on the side of the helix opposite to the hydrophobic face of the C-terminal portion (residues 15−29). In the crystal, glucagon exists as a trimer in which these hydrophobic portions can make intermolecular contact, thereby stabilizing the pattern of reversed amphipathic surfaces along the peptide chain. The crystal structure of a glucagon superagonist, [Lys[17,18], Glu[21]]glucagon (*17*), also shows a conformation very similar to that of glucagon, except for an extended α-helical conformation caused by the formation of a salt bridge between the side chains of Lys[18]

[†] This work was supported by grants from the U.S. Public Health Service (DK 21085 and EY12049).

[‡] Atomic coordinates for the minimized mean and final ensemble structures have been deposited with the Protein Databank at the RCSB under the file name 1NAU.

* To whom correspondence should be addressed. Phone: (520) 621-6332. Fax: (520) 621-8407. E-mail: hruby@u.arizona.edu.

[§] Present address: Department of Chemistry, The Scripps Research Institute, La Jolla, CA 92037.

10.1021/bi026629r CCC: $25.00
Published on Web 02/15/2003

and Glu[21] (*18*). The enhanced binding affinity and adenylate cyclase activity of the superagonist seem to result from increased helical content.

The solution structure of glucagon has been previously determined by nuclear magnetic resonance (NMR)[1] spectroscopy in the presence of perdeuterated dodecylphosphocholine micelles (*19*). The backbone conformation includes an unstructured region (residues 1−4), a predominantly extended segment (residues 5−9), one helixlike turn (residues 10−14), another stretch of extended chain (residues 14−17), and three turns of a distorted α-helix (residues 17−29). The orientation of the C-terminal helix with respect to the structural elements of the N-terminal region was not established. In aqueous solution, an overall extended random structure was observed for glucagon by one-dimensional NMR methods, though some residual structure was found for residues 22−26 (*20*). The effects of environmental conditions on the structure of glucagon are evident from the above structural differences, emphasizing the importance of having physiologically relevant conditions in conformational studies of glucagon and its analogues. More recently, the structure of the related peptide GLP-1-(7−36)-NH_2 was determined by NMR under nearly identical conditions in DPC micelles (*21*). This truncated form of glucagon-like peptide-1 (GLP-1) shows 50% sequence homology with glucagon (Figure 1) and is extended at the C-terminus by one residue and an amide cap. The solution structure is similar to glucagon, with four regions: a random-coil section (residues 1−6); an N-terminal α-helix (residues 7−14); a "loose helix" (residues 15−17); a C-terminal α-helix (residues 18−30). Again, no relationship was established between the two helices, although a helical distortion, leading to a helix phase shift, was suggested for residues 15−17 connecting the two helical segments (*21*). However, restrained molecular dynamics calculations led to an extensive α-helical structure from residues 6−28, with some flexibility around Gly-16 (*21*).

The potent glucagon antagonists [N^{α}-trinitrophenyl-His[1], homoArg[12]]glucagon (*9*), [desHis[1], Glu[9]]glucagon amide (*10*), and [desHis[1], desPhe[6], Glu[9]]glucagon amide (referred to as "glucagon antagonist" in this study; Figure 1) (*11*) have been developed by modification of the N-terminal region of the glucagon sequence, while the superagonist [Lys[17,18], Glu[21]]glucagon (*17*) was developed by modification of the C-terminal region. It has been demonstrated by X-ray crystallography (*18*) that the enhanced biological activity of the superagonist may result from an extended helical conformation in the C-terminal region. Yet there is little structural evidence to explain why modification of the N-terminal region converts glucagon into an antagonist, even though electrostatic interactions between His[1] and Asp[9] in glucagon and a coupled interaction of these two residues with the glucagon receptor have been suggested to play a role in the biological function of glucagon (*22*). A crystal structure is currently unavailable for the glucagon antagonist. Thus, to gain insight into the conformational differences which give it antagonistic activity, the solution structure of the glucagon antagonist was determined by homonuclear 2D-NMR spectroscopy in an aqueous solution of perdeuterated DPC micelles. DPC micelles have been widely used to solublize membrane proteins and peptides and to mimic the lipid bilayer environment of the membrane when determining their solution NMR structures (*19*, *21*, *23*, *24*). By contrast, studies of membrane proteins and peptides bound to lipid bilayers require solid-state NMR techniques (*25*). Multinuclear NMR relaxation studies (*26*) and molecular dynamics simulations (*27*) have shown that DPC micelles are realistic mimics of biological membranes. In addition, it has been shown that the conformation of DPC micelle-bound glucagon is very similar to that of lipid bilayer-bound glucagon (*28*). The structure of the glucagon antagonist found in our solution NMR study and the differences compared to various glucagon analogues may be relevant to their biological activities and may be useful to the further design of glucagon agonists and antagonists.

MATERIALS AND METHODS

Peptide Synthesis and Purification. The glucagon antagonist was synthesized using an Applied Biosystems ABI 431A automated peptide synthesizer and the HOBt-HBTU-Fmoc synthesis protocol (ABI version No. 1.01B). A Rink amide resin (0.25 mmol, substitution 0.7 mmol/g) was used, and the synthesis was carried out on a solid support using methodology very similar to that previously reported for glucagon analogues (*29*). A cleavage/deprotection mixture consisting of trifluoroacetic acid (18.0 mL), dimethylsulfide (0.5 mL), 1,2-ethanedithiol (0.5 mL), and anisole (1.0 mL) was chilled on ice. The resin-bound peptide (0.25 mmol) was placed in a disposable 50-mL polystyrene tube. The chilled cleavage mixture was added to the tube, and the resultant solution was bubbled with nitrogen for 2 min. The tube was capped and covered with aluminum foil, and the reaction mixture was stirred at room temperature for 2 h. The solution was filtered, and the resin was washed with trifluoroacetic acid (5 mL) and CH_2Cl_2 (2 × 5 mL). The combined solution was concentrated with a gentle stream of nitrogen to a volume of approximately 3 mL, and the peptide was precipitated with cold diethyl ether (40 mL). The peptide was centrifuged to remove the ether, washed with another 40 mL of diethyl ether, centrifuged, and dried *in vacuo*.

The peptide was purified by HPLC using a semipreparative VYDAC reverse-phase (C_{18}-bonded) HPLC column, with gradient elution (25−55% acetonitrile in 0.1% aqueous TFA over a 30 min interval) at a flow rate of 5.0 mL/ min. Approximately 5 mg of the crude peptide was injected onto the column each time, and the fraction containing the purified peptide was collected, followed by lyophilization. The extent of purity of the peptide was monitored by analytical HPLC, using an analytical VYDAC 218TPB-16 C_{18}-bonded column (4.6 × 250 mm), at 214, 254, and 280 nm. The molecular weight found by mass spectral analysis was 3211.5 (calcd, 3211.8). TLC: R_f 0.78 (A), 0.37 (B), 0.09 (C). HPLC: $k' = 4.83$ (10−90% acetonitrile in 0.1% aqueous TFA over a 40 min interval, flow rate 1.0 mL/min). Amino acid analysis: Asx 3.12 (3), Glx 3.94 (4), Ser 3.60 (4), Gly 1.19 (1). Arg

[1] Abbreviations: NMR, nuclear magnetic resonance; DPC, dodecylphosphocholine; CSD, chemical shift deviation; CSI, chemical shift index; rMD, restrained molecular dynamics; rmsd, root-mean-square deviation; DQF-COSY, double quantum filtered correlation spectroscopy; NOE, nuclear Overhauser effect; NOESY, nuclear Overhauser effect spectroscopy; TOCSY, total correlation spectroscopy; TPPI, time proportional phase incrementation; FID, free induction decay; GLP-1, glucagon-like peptide-1.

2.29 (2), Thr 3.10 (3), Ala 1.15 (1), Tyr 1.77 (2), Val 0.89 (1), Met 0.86 (1), Leu 2.16 (2), Phe 1.00 (1), Lys 1.00 (1).

NMR Spectroscopy. A 25 mg sample of the glucagon antagonist (7 mM) was dissolved in 0.6 mL of 50 mM sodium phosphate buffer (pH 6.0) containing 283 mM dodecylphosphocholine-d_{38} and 1 mM sodium azide (90% H_2O/10% D_2O). These experimental conditions are identical to those used for the structural determination of GLP-1 by NMR (*21*) and are similar to those (15 mM glucagon, 700 mM DPC-d_{38}, and pH 6.0) used for glucagon (*19*). In the case of glucagon under the above conditions, it was reported that mixed micelles contain about 40 DPC monomers and 1 peptide molecule, resulting in an equivalent molar mass of about 17 kD (*19*, *28*, *30*). All spectra were acquired on a Bruker AMX-500 spectrometer operating at a ^1H frequency of 500.13 MHz, using a proton-only water suppression 5 mm probe, with temperature regulation at 37 °C. All 2D spectra were acquired in the TPPI (*31*) mode with 4096 complex data points in t_2 and 750 real data points in t_1, using 64 repetitions for each t_1 value. A spectral width of 12 500 Hz was used in F_2 to minimize baseline distortions. In the F_1 dimension the spectral width was 6250 Hz. The H_2O signal was suppressed with 1.5 s of presaturation. Data were processed using Felix 2000 (Accelrys Inc., San Diego, CA). The FID data were zero-filled to 8192 complex data points before Fourier transformation, and the spectrum was truncated at both ends to give a spectral width of 6250 Hz in F_2. The size of the final matrix was 4096 (F_2) × 1024 (F_1) points, with the center point referenced to the water signal at 4.63 ppm.

For the DQF-COSY spectrum (*32*, *33*), an unshifted sine-bell window was used in both dimensions. H^N to H^α ^3J couplings were measured by analysis of the fingerprint region of the DQF-COSY spectrum. The matrix rows of each of the upper and lower halves of a cross-peak were summed to give an antiphase 1D spectrum, which was fitted using a 5-parameter nonlinear least-squares protocol (*34*) to a general antiphase doublet. The analysis yielded two independent determinations of the *J* coupling and line width for each cross-peak, one from the upper half and one from the lower half. Spin systems for each of the categories of amino acids were identified via the TOCSY spectrum (*35*−*37*), using a clean DIPSI-2rc mixing sequence (*38*), with a mixing time of 70 ms at an average spin-lock power level of 7.4 kHz. A skewed, 45°-shifted sine-bell window was used in both dimensions. The NOESY spectrum (*39*, *40*) established sequential connectivities and was obtained using presaturation during the mixing period of 150 ms, incorporating a 280 μs Hahn echo just before acquisition. A 90°-shifted sine-bell window was used in both dimensions. Cross-peak volumes for determination of distance restraints were measured using the Felix 2000 software.

Structure Calculations. The methods used for structure calculation have been described previously (*41*). Completely resolved cross-peaks between $H^\alpha(i)$ and $H^N(i + 3)$ of the C-terminal helix residues were used to calibrate the NOE volumes on the basis of the volume−distance relationship (volume $\propto r^{-6}$). The distance of 2.8 Å between these two hydrogen atoms in a standard α-helix (*42*) was used. The volumes of the assigned cross-peaks in the 2D NOESY spectrum were converted into upper distance bounds of 3.3, 4.0, 5.0, or 6.5 Å. Prior to the distance conversion, the volumes of cross-peaks arising from protons of methyl, degenerate methylene, or rapidly flipping aromatic rings were divided by the product of the number of protons involved in each NOESY dimension (*43*). For overlapped cross-peaks, one or two higher distance categories were used, depending on the qualitative estimate of the extent of overlap during the assignments. The sum of the van der Waals radii between nonbonded protons was used as the lower distance bound. Pseudoatoms were created for methyl protons, nonstereospecifically assigned methylene protons, or the protons on rapidly flipping aromatic rings. Pseudoatom corrections to their upper bound distances were then applied (*44*). For pseudoatoms of methyl groups, a correction of 0.5 Å was used to their upper bound distances (*45*, *46*). In addition to the distance restraints, ϕ dihedral angle restraints derived from $^3J_{HN-H\alpha}$ coupling constants were set to between −90 and −40° for $^3J_{HN-H\alpha} < 6$ Hz and to between −150 and −90° for $^3J_{HN-H\alpha} > 8$ Hz. For 6 Hz $< {}^3J_{HN-H\alpha} <$ 8 Hz, a negative ϕ dihedral angle restraint was used only if the sequential $H^\alpha(i-1) \rightarrow H^N(i)$ NOE was clearly stronger than the intraresidue $H^\alpha(i) \rightarrow H^N(i)$ NOE (*47*). Dihedral angles of 180° ± 5° for peptide bonds (ω) and dihedral angles of 180° ± 10° for glutamine (χ_4) and asparagine (χ_3) residues were also used to maintain the planarity of these bonds.

Use of the unshifted sine-bell window function, though enhancing the resolution, reduces the signal-to-noise ratio of the DQF-COSY spectrum, potentially making measurements of $^3J_{HN-H\alpha}$ couplings less accurate. To cross-validate the *J* coupling values, and to examine the effects of different coupling-derived ϕ dihedral angle restraints on the final structures, these couplings were alternatively determined using the DQF-COSY spectrum processed with only an exponential multiplier, using a line-broadening parameter of 0.5 Hz. The structures were recalculated using the identical NOE distance restraints but with the dihedral angle restraints derived from the couplings obtained with the exponential window function. Without the resolution enhancement, the *J* couplings for several residues (20, 24, 28, and 29) could not be determined due to resonance overlap. In the case of residue 16, though not overlapped, no reproducible measurements could be made. For couplings measurable in both spectra, most values are within the same classifications (*i.e.*, $J < 6$ Hz, $6 < J < 8$ Hz, or $J > 8$ Hz). The most appreciable differences occur for Ser^8, Asp^{15}, Arg^{17}, Val^{23}, Leu^{26}, and Met^{27}. In the case of Ser^8, two determinations of the couplings gave 6.19 and 5.99 Hz, respectively, in contrast to 5.65 and 5.56 Hz measured using the unshifted sine-bell window function. For Asp^{15}, larger values (8.15 and 8.06 Hz) were obtained from the spectrum processed with the 0.5 Hz line-broadening, compared to 7.09 and 7.13 Hz determined using resolution enhancement. In addition, Arg^{17}, Val^{23}, Leu^{26}, and Met^{27} were found to have couplings of less than 6 Hz, while couplings very close to 6 Hz were obtained using the unshifted sine-bell window function. Examination of the NMR structures calculated using the different ϕ dihedral angle restraints did not show significant differences in either the 15 lowest restraint energy ensemble structures or the minimized mean structure, though some minor structural variation was found. The backbone rmsd's for the different segments of the ensemble structures are 1.53 Å (residues 7−29), 1.74 Å (residues 2−5), 1.12 Å (residues 7−14), 0.47 Å (residues 15−18), and 0.28 Å

(residues 19−29). These values are similar to those (1.36, 1.68, 0.79, 0.54, and 0.33 Å) determined for the corresponding segments of the 15 ensemble structures calculated from the dihedral angle restraints derived using the unshifted sine-bell window function. The backbone rmsd's between the minimized mean structures from the two structure calculations using the different dihedral angle restraints are low: 0.57 Å for residues 7−29 (the overall alignment); 0.52 Å for residues 7−14 (the N-terminal helix); 0.27 Å for residues 15−18 (the hinge region); 0.12 for residues 19−29 (the C-terminal helix). The total energies of the structures calculated from the dihedral angle restraints derived from the couplings using the unshifted sine-bell window function are less. Therefore, use of these structures is preferred.

The hybrid distance geometry−simulated annealing protocol (*48*) was used to calculate the glucagon antagonist structures using the DGII (*49*) program within the software package INSIGHT II (Accelrys Inc., San Diego, CA). A total of 99 out of 100 embedded structures successfully passed the simulated annealing step and were minimized using the CVFF force field (Accelrys Inc.), which includes energy terms of bond lengths, bond angles, dihedral angles, out-of-plane interactions, van der Waals interactions, and electrostatic interactions. The 50 structures with the lowest penalty function were further refined by two rounds of restrained molecular dynamics (rMD) with the all-atom AMBER force field (*50*, *51*), using the standalone DISCOVER program (Accelrys Inc.). The AMBER force field includes all energy terms used in CVFF and an additional energy term for the hydrogen bonds. A 12.0 Å cutoff for nonbonded interactions and a distance-dependent dielectric constant (4*r*) were used. To minimize the charge−charge interaction artifacts, the partial atomic charges on the side chains of Asp, Glu, Arg, and Lys residues were reduced to ±0.2. A skewed biharmonic potential function was used for the experimental distance and dihedral angle restraints, with force constants of 25 kcal mol^{-1} $Å^{-2}$ and 100 kcal mol^{-1} rad^{-2}, respectively. After 100 steps of steepest descents minimization and 1000 steps of conjugate gradient minimization on the initial structures, an rMD equilibration at 500 K was then performed for 1.5 ps, during which a scale factor of 0.1 was applied to the experimental restraint force constants. During the next 2 ps, full values of the experimental restraint force constants were applied. A further 1 ps rMD simulation was run at 500 K, and the system was then cooled to 0 K over 3 ps. After another 1 ps at 0 K, 100 cycles of steepest descents and 2000 steps of conjugate gradient minimization wer performed. All calculations were performed on a Silicon Graphics Indy computer.

The NOESY spectra of the resulting minimized mean structure and the 15 lowest restraint energy structures of the ensemble were back-calculated using the Model module within the Felix 2000 program. A mixing time of 150 ms, a *z*-leakage rate of 2 Hz, a correlation time of 5 ns, and a distance cutoff of 7 Å were used. The calculated NOESY spectra were compared with the experimental spectrum, and the residual error between the real structure and the NMR structures was measured using the *R*-factor, defined (*52*) as follows:

$$R = \sum_i |(I^i_{\mathrm{exp}}) - (I^i_{\mathrm{cal}})| / \sum_i I^i_{\mathrm{exp}} \qquad (1)$$

Here I^i_{exp} and I^i_{cal} are the experimental and calculated NOE intensities of the i^{th} cross-peak. The back calculations were performed on a Silicon Graphics Octane computer.

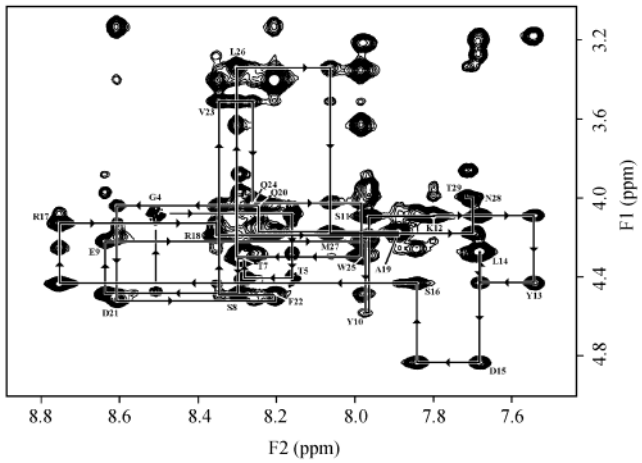

FIGURE 2: Fingerprint (H^N-H^α) region of the 150 ms NOESY spectrum of the glucagon antagonist in DPC micelles. Intraresidue H^N-H^α NOE cross-peaks are labeled by their one-letter code and residue number, and arrows indicate the connectivity path from N-terminus to C-terminus.

The ensemble-averaged coupling constants $\langle {}^3J_{\mathrm{HN-H\alpha}} \rangle$ were also back-calculated from the 15 lowest restraint energy structures of the ensemble. For each residue, the coupling constants ${}^3J^i_{\mathrm{HN-H\alpha}}$ were calculated for all 15 structures using the Karplus equation ${}^3J = 6.98 \cos^2\theta - 1.38 \cos\theta + 1.72$ (*53*), where θ is the $H^N-N-C^{\alpha-}H^\alpha$ dihedral angle. The ensemble-averaged coupling constants were then derived using the following equation:

$$\langle {}^3J_{\mathrm{HN-H\alpha}} \rangle = \sum_i {}^3J^i_{\mathrm{HN-H\alpha}} e^{-E_i/RT} / \sum_i e^{-E_i/RT} \qquad (2)$$

Here E_i is the total energy of the i^{th} structure, R is the gas constant, and T is the absolute temperature.

RESULTS AND DISCUSSION

Chemical Shift Assignments and Secondary Structure Analysis. At a nominal concentration of 7 mM the glucagon antagonist was insoluble in pH 6.0 phosphate buffer without DPC and gave an ^1H spectrum with extremely broad and weak resonances. With DPC micelles the solution was clear and the H^N peaks were narrow in the absence of resolution enhancement, increasing from about 5.5 Hz to 14 Hz (residues 5−17), remaining around 13−14 Hz for the rest of the molecule (residues 18−29). The ^1H chemical shifts of the glucagon antagonist, assigned using standard methods (*42*, *54*), are listed in the Supporting Information. Figure 2 shows the fingerprint region of the NOESY spectrum, with the sequential $H^N(i)-H^\alpha(i+1)$ NOE correlations diagrammed. As can be seen in Figure 2, the overall quality of the NOESY data is reasonably good, though the overlap of several H^α resonances made the assignment of some NOE cross-peaks difficult. The sequential NOE connectivity plots shown in Figure 3 summarize the evidence for secondary structural elements. Overall the evidence obtained from the coupling constants, chemical shift index (CSI) (*55*), and medium-range NOEs indicates the presence of a helical region (residues 8−13), an extended region (residues 15−16), and a second helix (residues 17−29). Interestingly, the

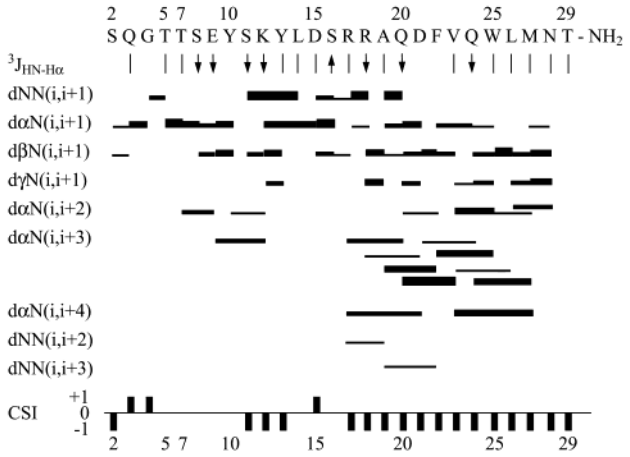

FIGURE 3: Diagram of H^N-H^α coupling constants, sequential and medium-range NOE connectivities, and H^α chemical shift index (CSI) for the glucagon antagonist in DPC micelles. Measured $^3J_{HN-H\alpha}$ coupling constants are indicated as follows: ↓, $J < 6$ Hz; |, 6 Hz $\leq J \leq$ 8 Hz; ↑, $J > 8$ Hz. The H^α CSI (*55*) was calculated using the random-coil values reported by Andersen *et al.* (*56*).

existence of the C-terminal helix is clear from the medium-range NOE and CSI patterns but not as evident from the $^3J_{HN-H\alpha}$ coupling constants, while the opposite holds for the N-terminal helix. This somewhat conflicting evidence may result from the considerable averaging of NMR parameters due to the relatively high flexibility of the peptide in solution. It should be noted that the coupling constants of several C-terminal residues are very close to 6 Hz. To avoid biasing the structure calculation, the coupling constant-derived dihedral angle restraints were used conservatively, and coupling constants were treated as beyond the helical region if one of the two determinations (see MATERIALS AND METHODS) of the *J* couplings exceeded 6 Hz. The ensemble-averaged *J* coupling constants which were back-calculated from the NMR ensemble structures show a good agreement with the medium-range NOE and CSI patterns for the C-terminal helix. In addition, the back-calculated NOESY spectra from the NMR structures reveal more $H^\alpha(i) \rightarrow H^N(i+3)$ NOE cross-peaks in the N-terminal helix than were observed, more consistent with the observed ^3J couplings for the N-terminal helix residues. Chemical shift deviations (CSDs) of the H^N and H^α protons can also be used to identify helical regions and breaks in the helical dipole (*56*), as shown in Figure 4. The H^N CSDs (*56*) in Figure 4a show clear evidence of two helical dipoles (residues 9−15 and 17−29), with a break between S16 and R17. The H^α CSDs in Figure 4b indicate an extended segment (residues 14−16) between two helical regions (residues 11−13 and 17−29).

Structure Determination. A total of 475 nonredundant NOE distance restraints were used, including 174 intraresidue, 137 sequential, 148 medium-range (2−4 residues), and 16 long-range restraints. The distribution of these restraints along the peptide chain is shown in Figure 5a. Dihedral angle restraints, obtained from $^3J_{HN-H\alpha}$ values, included seven "helical" Φ (−90 to −40°), one "extended" Φ (−150 to −90°), and three "negative" Φ (−179 to −1°) angle restraints. Because ^2H exchange data were unavailable, no hydrogen bond restraints were used. The total number of restraints was 486, giving an average of 18 restraints per

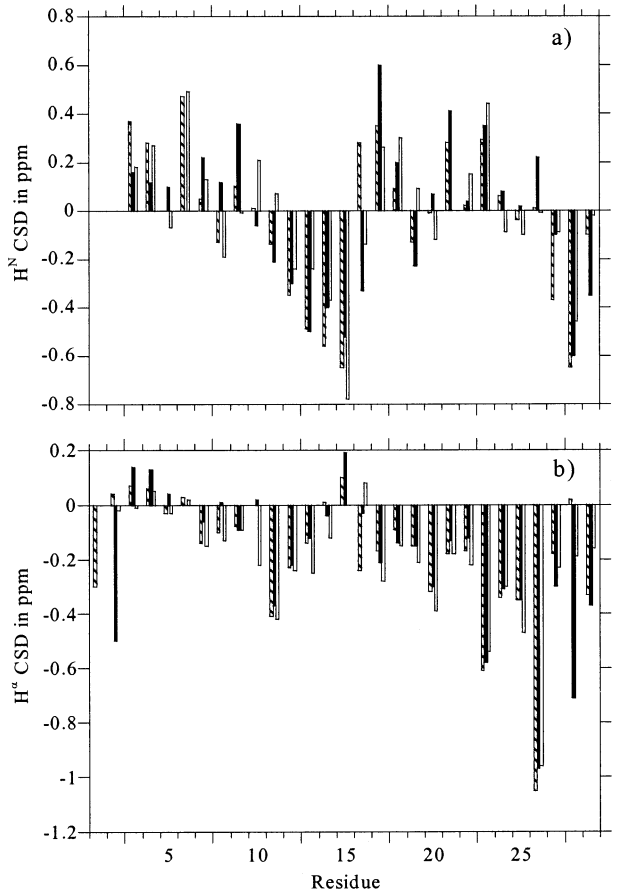

FIGURE 4: Chemical shift deviations (CSD) for (a) H^N and (b) H^α resonances compared to those of a random coil (*56*): hatched bars, glucagon; filled bars: the glucagon antagonist; open bars, GLP-1-(7−36)-NH_2.

residue. In addition, all of the peptide bond ω angles were restrained to 180 ± 5° to supplement the force field. The NOE restraints vary significantly along the chain and are most numerous for two regions at the polypeptide, from residues 9 to 14 and from residues 17 to 27.

The 15 structures with the lowest restraint energies after rMD refinement were used to represent the structure of the glucagon antagonist in DPC micelles. Statistics for these 15 structures are shown in Table 1. The average restraint violation energy is low (2.8 ± 0.4 kcal mol^{-1}), with an average maximum NOE distance violation of 0.14 Å and an average maximum dihedral angle violation of 0.3° (Table 1). The *R*-factors for the 15 ensemble structures and the minimized mean structure were calculated for the 396 completely resolved cross-peaks to be 0.33 ± 0.09 and 0.16, respectively, indicating a good agreement between our NMR structures and the experimental NOESY data. The backbone and non-hydrogen atom rmsd's of the 15 structures with respect to the mean coordinates for each residue are plotted in Figure 5b,c, respectively. As can be seen, the rmsd values are largest near the N-terminus and decrease steadily along the polypeptide toward the C-terminus. The angular order parameters $S(\phi)$ and $S(\psi)$ of the backbone dihedral angles (ϕ, ψ) (*57*) are shown in Figure 6a. An increase in the order parameters is evident from the N- to the C-terminus, indicating that the polypeptide becomes more structured. Figure 6b depicts the corresponding Ramachandran plot which shows a predominantly helical structure. The ensemble

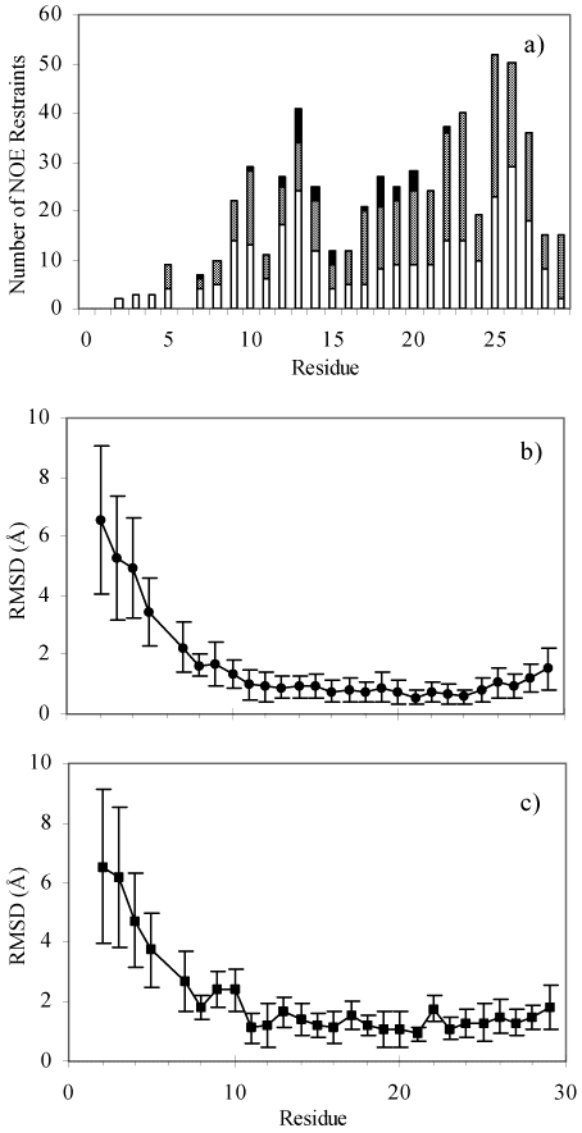

FIGURE 5: (a) Number of NOE distance restraints by residue for the glucagon antagonist. Each column shows the sequential restraints (i, $i + 1$; open), medium range restraints (i, $i + 2-4$; hatched), and long-range restraints (i, $i + >4$; filled). (b) and (c) Atomic rmsd by residue for the 15 final structures with the lowest restraint energy, aligned on residues 7−29 with the mean structure using backbone atoms (b) or all non-hydrogen atoms (c).

Table 1: Structural Statistics

	final 15 structs	minimized mean
rms deviation from 475 NOE dist restraints (Å)	0.015 ± 0.001	0.016
rms deviation from 11 backbone ϕ angle restraints (deg)	0.099 ± 0.187	0
NOE dist restraint violations		
>0.01 Å	33.7 ± 3.8	32
>0.10 Å	2.7 ± 1.0	3
max dist violation (Å)	0.14 ± 0.02	0.16
dihedral angle violations		
>0.1°	0.6 ± 0.7	0
>1°	0.1 ± 0.4	0
max dihedral violation (deg)	0.3 ± 0.6	0
rms deviation from ideal geometry[a]		
bond lengths (Å) (443)	0.0047 ± 0.0001	0.0048
bond valence angles (deg) (784)	1.51 ± 0.06	2.76
out-of-plane angles (deg) (93)	2.02 ± 0.20	2.05
AMBER energies (kcal/mol)		
restraint[b]	2.8 ± 0.4	3.2
bond stretching	3.4 ± 0.2	3.4
bond angles	24.1 ± 1.9	68.4
dihedral angles	22.4 ± 1.5	22.7
planarity	0.9 ± 0.1	0.9
van der Waals[c]	−82.2 ± 4.7	−86.4
electrostatic[d]	−73.0 ± 1.8	−74.2
tot.	−117.7 ± 6.0	−77.9

	atomic rms deviation (Å)[e]	
	backbone atoms (N, C^α, C')	all non-hydrogen atoms
final 15 structs vs mean	1.12 ± 0.26	1.63 ± 0.28
final 15 structs vs minimized mean	1.20 ± 0.67	1.88 ± 0.61
mean vs minimized mean	0.81	1.12

[a] Derived from the rMD calculations using the AMBER force field in DISCOVER. [b] Calculated with force constants of 25 kcal mol^{-1} $Å^{-2}$ and 100 kcal mol^{-1} rad^{-2} for the NOE distance and dihedral angle restraints, respectively. [c] Calculated with the Lennard-Jones potential using the AMBER force field and a 12 Å cutoff. [d] Calculated with a distance-dependent dielectric constant ($\epsilon = 4r$). [e] Calculated for residues 7−29 for the final 15 structures. The mean structure was the average of the final 15 structures that were best fit to each other using the atoms of N, C^α, and C' of residues 7−29. The coordinates of disordered residues 2−5 were then replaced with those of the corresponding residues in the closest one of the 15 aligned structures. The minimized mean was obtained by restrained minimization of the mean structure.

of 15 structures is illustrated in Figure 7, aligned on residues 7−29 (Figure 7a) to show the overall structure, and on residues 7−14 (Figure 7b) and 17−29 (Figure 7c) to show the N-terminal and C-terminal helices, respectively.

It is noteworthy that a Kabsch and Sander (*58*) analysis of the 15 final structures using the Insight II software indicates five general regions for the glucagon antagonist in DPC micelles: a region of random coil at the N-terminus (residues 2−7); an N-terminal helical region (residues 7−12); a turn (residues 12−14); another random coil region (residues 14−17); a C-terminal helix (residues 17−29). These conclusions are consistent with the qualitative evidence from NOEs (Figure 3), which show extensive helical contacts (i, $i + 3$ and i, $i + 4$) in the C-terminal helix (residues 17−27). In addition, the H^N and H^α CSDs (Figure 4) indicate two separate helical runs (residues 9−13 and 17−29) broken by a single extended residue (*15*). Similarly the H^N-H^α J couplings (Figure 3) show two helical regions (residues 8−12 and 18−24) and a single extended residue (*16*). The common trends evident in H^N line widths (data not shown), the number of observed NOEs per residue (Figure 5), and the angular order parameters of the calculated structures (Figure 6) all indicate that the structure is well defined for the two helical regions (residues 8−13 and 18−29), less defined for the "hinge" region (residues 15−17), and more or less random for the N-terminal region (residues 2−7). More importantly, alignment of the calculated structures (Figure 7) shows that the two helical regions exist in a well-defined relationship, having roughly a 90° angle between the helix axes. This relationship is defined experimentally by a cluster of 13 long-range NOEs between residues 10−13 and residues 16−18. While backbone rmsd's for the individual helical regions are considerably smaller (Figure 7b,c), the backbone rmsd for the entire molecule, excluding the unstructured N-terminus, is still quite low (Figure 7a). This is the first example of a glucagon analogue in DPC micelles with an organized overall structure which includes both sides of the "hinge" region.

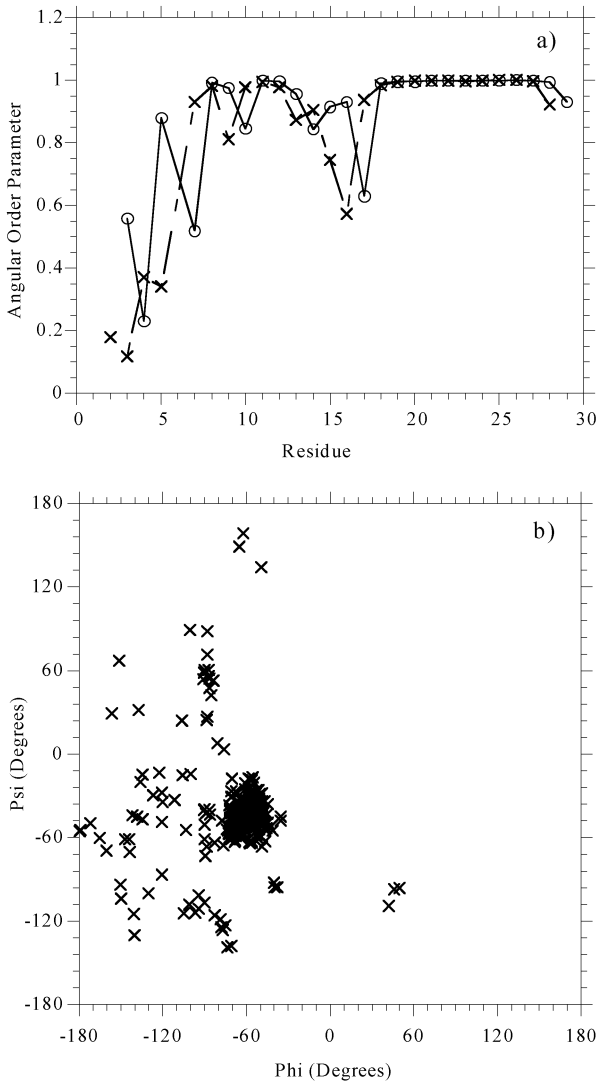

FIGURE 6: (a) Angular order parameters for ϕ (open circles) and ψ (crosses) for all residues of the glucagon antagonist. The angular order parameters for a given dihedral angle α are defined as $S(\alpha) = N^{-1}|\Sigma_j \alpha_j|$, where $j = 1, \ldots N$ indicate the various structures and α_j is a 2D unit vector whose phase is equal to the dihedral angle (*57*). (b) Ramachandran plot for residues 7−28, calculated for the 15 structures with the lowest restraint energy.

A consensus conformation for the hinge region (Figure 8) was obtained by selecting the 12 most similar conformations of the 20 lowest restraint energy structures. In this ensemble, five of the structures have a bifurcated hydrogen bond between the backbone carbonyl of K12 and the H^N of L14 and D15, while four have a hydrogen bond only to the H^N of D15 and two have a hydrogen bond only to the H^N of L14. These observations are consistent with the presence of a β-turnlike conformation in this segment of the glucagon antagonist structure. Although this β-turn structure does not readily fit the criteria for any specific β-turn structure, examination of the different backbone conformations suggests this turnlike structure is centered in the vicinity of the Y13 and L14 residues and most closely resembles a type III β-turn. This nonconventional turn structure is consistent with the long-range NOEs observed between the regions 12−15 and 17−20. The turnlike structure allows long-range interactions between these two segments, as seen in the ensemble of 15 structures (Figure 7). The short N-terminal helix is connected by the hinge region to the longer C-terminal helix (3 turns), where the angle between the two helix axes is close to 90°.

Conformational Comparison of Glucagon, the Glucagon Antagonist, and GLP-1-(7−36)-NH_2. Because detailed structural information for glucagon and glucagon analogues is limited, it is useful to compare the CSD patterns, which can easily be calculated from the chemical shift assignments. It must be pointed out that currently available H^α and H^N proton chemical shift data for calculating CSD/CSI values (*55*, *56*) were obtained in water in the absence of DPC micelles so that an inconsistency between the shift values in the two different environments may occur (*59*). In this study, however, the chemical shifts of glucagon and the glucagon analogues were all measured in DPC micelles, making a meaningful comparison between their CSD values possible. As illustrated by Figure 4a,b, there is a great deal of similarity in the CSDs between glucagon, the glucagon antagonist, and the glucagon homologue GLP-1-(7−36)-NH_2, implying similar secondary structures in DPC micelles. The only significant differences occur in the hinge region, where positive H^α CSDs are observed for D15 in glucagon and the glucagon antagonist but no H^α CSD is observed for E15 in GLP-1-(7−36)-NH_2. Furthermore, glucagon shows a positive H^N CSD for S16, while the glucagon antagonist and GLP-1-(7−36)-NH_2 show negative H^N CSDs for S16 and G16, respectively. These differences could reflect differences in the hinge region and a different starting point for the C-terminal helix, but overall the CSD patterns are extremely similar for glucagon and the two analogues.

If one views as a conceptual starting point the glucagon antagonist as a single continuous helix, it would be amphipathic with the hydrophobic and hydrophilic sides reversed between the N-terminal (residues 2−16) and C-terminal (residues 17−29) regions. The deletion of Phe^6 places Thr^5 of the glucagon antagonist in the location of Phe^6 in the helical wheel diagram (Figure 9); otherwise the same reversed amphipathic nature is seen as in the crystal structure of glucagon (*16*). The solution structure of the glucagon antagonist in DPC micelles can be viewed as an unraveling of this hypothetical extended helix by rotating the C-terminal portion by 180° about the helix axis (a helix "phase shift") and then bending in the "hinge" region to place the two hydrophobic surfaces together in the angle of a 90° bend. In this region there are two hydrophobic clusters: the N-terminal hydrophobic surface consisting of the side chains of Y10, Y13, and L14 and the C-terminal hydrophobic surface composed of the side chains of F22, V23, W25, L26, and M27. In many of the calculated structures there is a stacking of the aromatic rings of Y13 and F22, joining the two hydrophobic clusters. On the convex, hydrophilic face of the molecule there are two salt bridges implied from the close approach of side chains in the calculated structures: D15 to R18; R17 to D21. The first of these maps onto the interface between the two amphipathic helical portions, and the second is within the hydrophilic face of the C-terminal amphipathic helix.

The solution structure of the glucagon antagonist obtained in DPC micelles in our study is significantly different from the glucagon X-ray crystal structure (*16*). It also differs from the glucagon solution structure in the absence of DPC micelles observed by one-dimensional NMR methods (*20*), which can be attributed to the significant differences in the

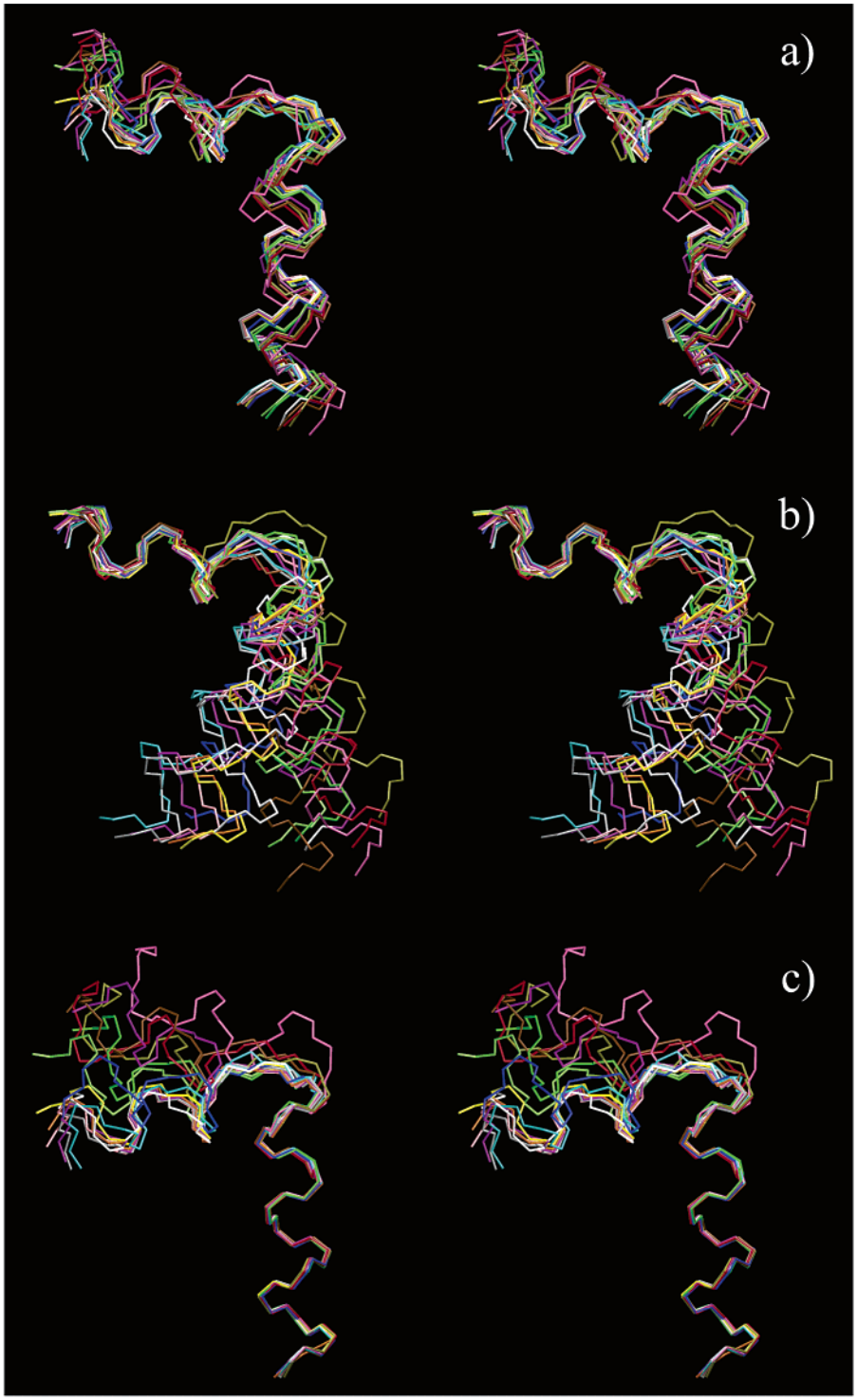

FIGURE 7: Stereodiagrams of the 15 calculated structures for the glucagon antagonist with the lowest restraint energy, aligned on backbone atoms of residues (a) 7−29 (rmsd = 1.36 Å), (b) 7−14 (rmsd = 0.79 Å), and (c) 17−29 (rmsd = 0.42 Å). The backbone atoms of residues 7−29 only are shown. The figure was produced using VMD (*63*) and Raster3D (*64*).

experimental conditions. In a comparison of the glucagon X-ray crystal structure and our glucagon antagonist NMR mean structure, the two helical segments (residues 7−14 and residues 19−27) gave backbone rmsd's of 0.78 and 0.69 Å, respectively, which implies the helical stability of these two segments. However, in contrast to the single continuous helix (residues 6−29), and the pattern of the reversed amphipathic surfaces along the peptide chain (*16*), a helical unraveling in the vicinity of the hinge region connecting the two helical segments and a resulting helix phase shift are observed in our glucagon antagonist NMR structure. Due to the absence of crystal packing forces in solution, the favorable intramolecular hydrophobic interactions between the two helical segments of the glucagon antagonist in DPC micelles may drive this unusual folding around the hinge region. Nonetheless, these hydrophobic interactions resulting from the helix phase shift seem to be insufficient to stabilize the structure observed for the glucagon antagonist. In aqueous solution in the absence of micelles, the structure of the glucagon antagonist observed in DPC micelles may be unstable due

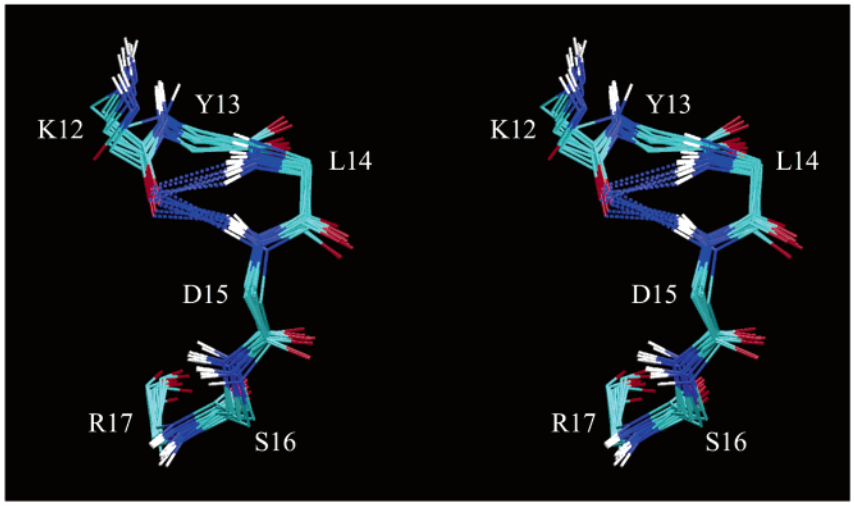

FIGURE 8: Stereodiagram of 12 consensus structures for the glucagon antagonist chosen from the 20 structures with the lowest restraint energy, showing expansion of the hinge region (residues 12−17, rmsd = 0.36 Å). The carbon atoms are shown in cyan, nitrogen atoms in blue, oxygen atoms in red, and hydrogen atoms in white. Hydrogen bonds are indicated by the blue dashed lines. The figure was produced using VMD (*63*) and Raster3D (*64*).

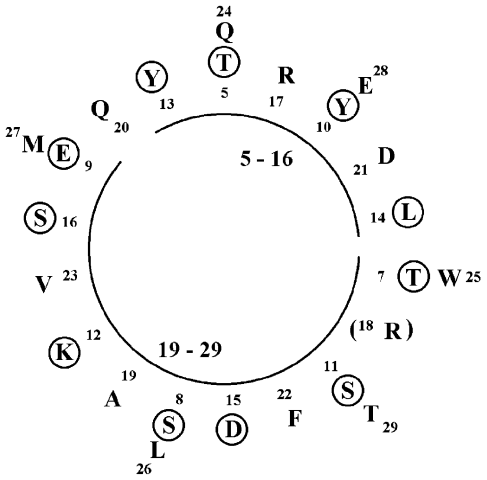

FIGURE 9: Helical wheel for the glucagon antagonist, omitting residues 2−4, viewed as a continuous α-helix. One-letter amino acid codes in the N-terminal amphipathic region are circled (5−16). The N-terminal hydrophobic surface is indicated by the arc labeled 5−16, and the C-terminal hydrophobic surface is represented by the arc labeled 19−29.

to exposure to water of the hydrophobic cluster resulting from the helix phase shift. This is supported by evidence for an overall extended random structure of glucagon in aqueous solution without micelles (*20*). Therefore, the favorable interactions between the hydrophobic surfaces of the glucagon antagonist and the hydrocarbon chains of the micelles appear to play an important role in stabilizing our glucagon antagonist NMR structure. Under the more physiologically relevant conditions in our study, compared to the conditions in the crystal state or in the absence of micelles, the derived structural information can be assumed to be more applicable.

Structure−Activity Relationships. The observed helical distortion and resulting helix phase shift in the hinge region of the glucagon antagonist found in our study may have some important biological significance. An extended hydrophobic cluster along the inner surface and a hydrophilic surface along the outer surface of the L-shaped structure is formed due to the helix phase shift, which presumably favors hydrophobic/hydrophilic interactions of the peptide with the membrane and receptor. In addition, the helical distortion may result in some important backbone dynamics properties of the glucagon antagonist. The cooperative backbone motions of the glucagon antagonist are evident from the 15 ensemble structures in Figure 7. It can be seen that the two helical segments are relatively rigid, while the flexibility of the hinge region allows a range of relative orientations of these two segments. The various relative orientations accessible to the two helices may facilitate the required multiple contacts of the peptide with a discontinuous domain, consisting of the two segments (residues 103−117 and 126−137) in the N-terminal region and another segment (residue 206−219) in the first extracellular (1e) loop of the glucagon receptor, which are found to be critical in binding and/or signaling (*60*). A similar helical distortion and phase shift was also suggested for GLP-1-(7−36)-NH_2 in DPC micelles due to the presence of the helix-destabilizing residue Gly^{16} (*21*) in the region corresponding to the hinge in the glucagon antagonist. It has been further suggested that Ser^{16} in glucagon makes it more difficult to accomplish the helix distortion, which may be responsible for the much poorer binding affinity of glucagon for the GLP-1 receptor (*21*). The observation of the same helix phase shift in the glucagon antagonist, which differs from glucagon primarily at only a few residues near the N-terminal end, makes this unlikely. Moreover, this phase shift may also occur in glucagon in DPC micelles, as implied by the similarity of the H^{α} CSD patterns of glucagon and the glucagon antagonist near the hinge region (Figure 4) and the reasonably low average backbone rmsd (1.28 Å) obtained in a comparison of the five lowest energy structures of glucagon (*19*) with the minimized mean structure of the glucagon antagonist for residues 15−17.

A comparison of the side chain conformations of the mutated residue Glu^9 observed in our glucagon antagonist NMR ensemble structures with those of Asp^9 in glucagon (*19*) may explain the biological effects of the structural alteration. Due to the rotation around χ_2 for Glu^9 in the glucagon antagonist, a much larger region of space appears to be accessible to the carboxylate group (and thus the charge) than to that of Asp^9 in glucagon, even though their χ_1 rotamer population distributions are similar. This presum-

ably increases the entropy cost for interaction between Glu^9 in the glucagon antagonist and complementary residues in the glucagon receptor. It was suggested that Arg^{202} in the 1e loop of the glucagon receptor, which is critical for both binding and signaling, interacts with several possible residues including Asp^9 in glucagon (*60*). The unfavorable interactions due to the above effects between Glu^9 in the glucagon antagonist and Arg^{202} in the glucagon receptor may rationalize the effects of the mutation from Asp^9 in glucagon to Glu^9 in the glucagon antagonist and also other glucagon analogues (*22*). Unfortunately, due to the lack of structure observed by NMR for the N-terminal ends of both glucagon (*19*) and the glucagon antagonist, it is beyond the capability of solution NMR techniques to provide any rationalization for the biological effects of electrostatic interactions between His^1 and Asp^9 in glucagon, as suggested in an earlier study (*22*). This technical limitation also makes it extremely difficult to analyze the effects of the deletions of His^1 and Phe^6 on the structure of the glucagon antagonist in this study.

With regard to binding of peptide ligands to their membrane receptors, a two-step model has been proposed which is thought to kinetically favor binding more than a single-step binding model (*61*). This model or a similar one has been used to analyze the binding of ligands to type B receptors in the GPCR superfamily (*19*, *21*, *60*, *62*). With application of such a model, nonspecific interactions between the hydrophobic C-terminal helix of the glucagon antagonist and the membrane would occur as the first step, followed by the two-dimensional diffusion of the peptide until it binds to the N-terminal tail and the 1e loop of the glucagon receptor in the second step. Conformational differences between the antagonist and glucagon near the N-terminus may then result in unfavorable interactions between the antagonist and the receptor, which do not lead to activation.

In conclusion, the NMR solution structure of the glucagon antagonist [$desHis^1$, $desPhe^6$, Glu^9]glucagon amide in DPC micelles shows a well-defined spatial relationship between the N-terminal and C-terminal helices, unlike the NMR solution structures of glucagon (*19*) and other glucagon homologues (*21*). The previous lack of definition of the overall structure of glucagon may be due simply to the failure to observe sufficient long-range NOE interactions. Further study, including the investigation of backbone dynamics, will be required to define any structural differences between the glucagon antagonist and glucagon itself which could explain the dramatic difference in biological activity.

ACKNOWLEDGMENT

We thank Professor Kurt Wüthrich for sending us the coordinates of the glucagon NMR structures in DPC micelles in solution, which were recalculated using the previous experimental data in reference (*19*) by Francesco Fiorito. We also acknowledge many invaluable discussions on structure calculations with Dr. Wayne J. Fairbrother of Genentech, Inc., as well as many helpful discussions of hormone structure−activity relationships with Devendra B. Trivedi.

SUPPORTING INFORMATION AVAILABLE

Chemical shift assignments for the glucagon antagonist [$desHis^1$, $desPhe^6$, Glu^9]glucagon amide. This material is available free of charge via the Internet at http://pubs.acs.org.

REFERENCES

1. Johnson, M. E. M., Das, N. M., Butcher, F. R., and Fain, J. N. (1972) *J. Biol. Chem. 24*, 3229−3235.
2. Farah, A. E. (1983) *Phamacol. Rev. 35*, 181−217.
3. McGarry, J. D., and Foster, D. W. (1980) *Annu. Rev. Biochem. 49*, 395−420.
4. Unger, R. H., and Orci, L. (1975) *Lancet 1*, 14−16.
5. Unger, R. H. (1978) *Metabolism 27*, 1691−1709.
6. Hruby, V. J. (1982) *Mol. Cell. Biochem. 44*, 49−64.
7. Hruby, V. J., Krstenansky, J. L., Gysin, B., Pelton, J. T., Trivedi, D., and McKee, R. L. (1986) *Biopolymers 25*, S135−S155.
8. Hruby, V. J. (1997) in *Principles of Medical Biology. Molecular and Cellular Endocrinology* (Bittar, E. E., and Bittar, N., Eds.) pp 387−403, JAI Press, Greenwich, CT.
9. Bregman, M. D., Trivedi, D., and Hruby, V. J. (1980) *J. Biol. Chem. 255*, 11725−11731.
10. Unson, C. G., Andreu, D., Gurzenda, E. M., and Merrifield, R. B. (1987) *Proc. Natl. Acad. Sci. U.S.A. 84*, 4083−4087.
11. Azizeh, B. Y., Van Tine, B. A., Sturm, N. S., Hutzler, A. M., David, C., Trivedi, D., and Hruby, V. J. (1995) *Bioorg. Med. Chem. Lett. 5*, 1849−1852.
12. Johnson, D. G., Goebel, C. A., Hruby, V. J., Bregman, M. D., and Trivedi, D. (1982) *Science 215*, 1115−1116.
13. Unson, C. G., Gurzenda, E. M., and Merrifield, R. B. (1989) *Peptides 10*, 1171−1177.
14. Van Tine, B. A., Azizeh, B. Y., Trivedi, D., Jason, R. P., Houslay, M. D., Johnson, D. G., and Hruby, V. J. (1996) *Endocrinology 137*, 3316−3322.
15. Korn, A. P., and Ottensmeyer, F. P. (1983) *J. Theor. Biol. 105*, 403−425.
16. Sasaki, K., Dockerill, S., Adamiak, D. A., Tickle, I. J., and Blundell, T. (1975) *Nature 257*, 751−757.
17. Krstenansky, J., Trivedi, D., Johnson, D., and Hruby, V. J. (1986) *J. Am. Chem. Soc. 108*, 1696−1698.
18. Sturm, N. S., Lin, Y., Burley, S. K., Krstenansky, J. L., Ahn, J.-M., Azizeh, B. Y., Trivedi, D., and Hruby, V. J. (1998) *J. Med. Chem. 41*, 2693−2700.
19. Braun, W., Wider, G., Lee, K. H., and Wüthrich, K. (1983) *J. Mol. Biol. 169*, 921−948.
20. Boesch, C., Bundi, A., Oppliger, M., and Wüthrich, K. (1978) *Eur. J. Biochem. 91*, 209−214.
21. Thornton, K., and Gorenstein, D. G. (1994) *Biochemistry 33*, 3532−3539.
22. Unson, C. G., Macdonald, D., Ray, K., Durrah, T. L., and Merrifield, R. B. (1991) *J. Biol. Chem. 266*, 2763−2766.
23. Karslake, C., Piotto, M. E., Pak, Y. K., Weiner, H., and Gorenstein, D. G. (1990) *Biochemistry 29*, 9872−9878.
24. Arora, A., Abildgaard, F., Bushweller, J. H., and Tamm, L. K. (2001) *Nat. Struct. Biol. 8*, 334−338.
25. Brown, M. F. (1996) in *Biological Membranes-A Molecular Perspective from Computation and Experiment* (Merz, K. M., Jr., and Roux, B., Eds.) pp 175−252, Birkhäuser, Boston, MA.
26. Beswick, V., Guerois, R., Cordier-Ochsenbein, F., Coïc, Y.-M., Huynh-Dinh, T., Tostain, J., Noël, J.-P., Sanson, A., and Neumann, J.-M. (1998) *Eur. Biophys. J. 28*, 48−58.
27. Wong, T. C., and Kamath, S. (2002) *J. Biomol. Struct. Dyn. 20*, 39−57.
28. Bösch, C., Brown, L. R., and Wüthrich, K. (1980) *Biochim. Biophys. Acta 603*, 298−312.
29. Ahn, J.-M., Madeiros, M., Trivedi, D., and Hruby, V. J. (2001) *J. Pept. Res. 58*, 151−158.
30. Wider, G., Lee, K. H., and Wüthrich, K. (1982) *J. Mol. Biol. 155*, 367−388.
31. Marion, D., and Wüthrich, K. (1983) *Biochem. Biophys. Res. Commun. 113*, 967−974.
32. Piantini, U., Sørensen, O. W., and Ernst, R. R. (1982) *J. Am. Chem. Soc. 104*, 6800−6801.
33. Rance, M., Sørensen, O. W., Bodenhausen, G., Wagner, G., Ernst, R. R., and Wüthrich, K. (1983) *Biochem. Biophys. Res. Commun. 117*, 479−485.
34. Press, W. H., Vetterling, W. T., and Teukolsky, S. A. (1988) *Numerical Recipes in C. The Art of Scientific Computing*, Cambridge University Press, New York.
35. Braunschweiler, L., and Ernst, R. R. (1983) *J. Magn. Reson. 53*, 521−528.
36. Bax, A., and Davis, D. G. (1985) *J. Magn. Reson. 65*, 355−360.
37. Davis, D. G., and Bax, A. (1985) *J. Am. Chem. Soc. 107*, 2820−2821.

38. Cavanagh, J., and Rance, M. (1992) *J. Magn. Reson. 96*, 670−678.
39. Jeener, J., Meier, B. H., Bachmann, P., and Ernst, R. R. (1979) *J. Chem. Phys. 71*, 4546−4553.
40. Macura, S., and Ernst, R. R. (1980) *Mol. Phys. 41*, 95−117.
41. Jacobsen, N. E., Abadi, N., Sliwkowski, M. X., Reilly, D., Skelton, N. J., and Fairbrother, W. J. (1996) *Biochemistry 35*, 3402−3417.
42. Wüthrich, K. (1986) *NMR of Proteins and Nucleic Acids*, Wiley, New York.
43. Yip, P. (1990) *J. Magn. Reson. 90*, 382−383.
44. Wüthrich, K., Billeter, M., and Braun, W. (1983) *J. Mol. Biol. 169*, 949−961.
45. Tropp, J. (1980) *J. Chem. Phys. 72*, 6035−6043.
46. Koning, T. M. G., Boelens, R., and Kaptein, R. (1990) *J. Magn. Reson. 90*, 111−123.
47. Clubb, R. T., Ferguson, S. B., Walsh, C. T., and Wagner, G. (1994) *Biochemistry 33*, 2761−2772.
48. Nilges, M., Clore, G. M., and Gronenborn, A. M. (1988) *FEBS Lett. 239*, 317−324.
49. Havel, T. F. (1991) *Prog. Biophys. Mol. Biol. 56*, 43−78.
50. Weiner, S. J., Kollman, P. A., Case, D. A., Singh, U. C., Ghio, C., Alagona, G. S., Profeta, J., and Weiner, P. (1984) *J. Am. Chem. Soc. 106*, 765−784.
51. Weiner, S. J., Kollman, P. A., and Case, D. A. (1986) *J. Comput. Chem. 7*, 230−252.
52. Thomas, P. D., Basus, V. J., and James, T. L. (1991) *Proc. Natl. Acad. Sci. U.S.A. 88*, 1237−1241.
53. Wang, A. C., and Bax, A. (1996) *J. Am. Chem. Soc. 118*, 2483−2494.
54. Cavanagh, J., Fairbrother, W. J., Palmer, A. G., III, and Skelton, N. J. (1996) *Protein NMR Spectroscopy Principles and Practice*, Academic Press, New York.
55. Wishart, D. S., Sykes, B. D., and Richards, F. M. (1992) *Biochemistry 31*, 1647−1651.
56. Andersen, N. H., Neidigh, J. W., Harris, S. W., Lee, G. M., Liu, Z. H., and Tong, H. (1997) *J. Am. Chem. Soc. 119*, 8547−8561.
57. Hyberts, S., Goldberg, M. S., Havel, T. F., and Wagner, G. (1992) *Protein Sci. 1*, 736−751.
58. Kabsch, W., and Sander, C. (1983) *Biopolymers 22*, 2577−2637.
59. Neidigh, J. W., Fesinmeyer, R. M., Prickett, K. S., and Andersen, N. H. (2001) *Biochemistry 40*, 13188−13200.
60. Unson, C. G., Wu, C.-R., Jiang, Y., Yoo, B., Cheung, C., Sakmar, T. P., and Merrifield, R. B. (2002) *Biochemistry 41*, 11795−11803.
61. Adam, G., and Delbrück, M. (1968) in *Structural Chemistry and Molecular Biology* (Rich, A., and Davidson, N., Eds.) pp 198−215.
62. Inooka, H., Ohtaki, T., Kitahara, O., Ikegami, T., Endo, S., Kitada, C., Ogi, K., Onda, H., Fujino, M., and Shirakawa, M. (2001) *Nat. Struct. Biol. 8*, 161−165.
63. Humphrey, W., Dalke, A., and Schulten, K. (1996) *J. Mol. Graphics 14*, 33−38.
64. Merritt, E. A., and Bacon, D. J. (1997) *Methods Enzymol. 277*, 505−524.

BI026629R